

# Generating quantum entanglement between macroscopic objects with continuous measurement and feedback control

Daisuke Miki,<sup>1</sup> Nobuyuki Matsumoto,<sup>2</sup> Akira Matsumura,<sup>1</sup> Tomoya Shichijo,<sup>1</sup>

Yuuki Sugiyama,<sup>1</sup> Kazuhiro Yamamoto,<sup>1,3</sup> Naoki Yamamoto,<sup>4,5</sup>

<sup>1</sup>*Department of Physics, Kyushu University, 744 Motoooka, Nishi-Ku, Fukuoka 819-0395, Japan*

<sup>2</sup>*Department of Physics, Faculty of Science, Gakushuin University, 1-5-1, Mejiro, Toshima, Tokyo, 171-8588 Japan*

<sup>3</sup>*Research Center for Advanced Particle Physics, Kyushu University,  
744 Motoooka, Nishi-ku, Fukuoka 819-0395, Japan*

<sup>4</sup>*Quantum Computing Center, Keio University, Hiyoshi 3-14-1, Kohoku, Yokohama 223-8522, Japan and*

<sup>5</sup>*Department of Applied Physics and Physico-Informatics,  
Keio University, Hiyoshi 3-14-1, Kohoku, Yokohama 223-8522, Japan \**

(Dated: October 25, 2022)

This study is aimed at investigating the feasibility of generating quantum entanglement between macroscopic mechanical mirrors in optomechanical systems while under continuous measurement and feedback control. We carefully derive a covariance matrix for mechanical mirrors in a steady state, employing the Kalman filtering problem with an assumed dominant cavity photon dissipation, such that the common and differential modes of the mirrors are squeezed by the action of measuring the output light beams. We demonstrate that entanglement between the mechanical mirrors is generated when the states of the common and differential modes are squeezed with high purity in an asymmetric manner. Our results also show that quantum entanglement between 7 mg mirrors is achievable in the short term.

## I. INTRODUCTION

Cavity optomechanics deals with the coupled dynamics of the oscillating end mirrors of cavities (mechanical oscillators) and the optical mode therein. This field has the potential to reveal the boundary between the classical and the quantum world [1–6]. The quantum states of mechanical oscillators can be achieved by quantum control through interaction with optical cavity modes, whereas mechanical oscillators lose quantum coherence owing to thermal fluctuations. The technique of continuous measurement cooling shows the potential to achieve the quantum states of macroscopic mechanical oscillators [4, 6, 7]. Ref. [8] demonstrated cooling a mechanical oscillator to the ground state through cavity detuning and feedback control. Moreover, optomechanical systems are helpful in generating entanglements. The authors in Refs. [9, 10] considered the detectability of entanglement between the optical cavity mode and the mechanical oscillator in the ground state. Refs. [11–13] showed that the generation of quantum entanglement between nanoscale objects was realized experimentally. Recently, cavity optomechanics has attracted significant interest as a possible field for investigating the quantum nature of gravity through tabletop experiments [14–20]. Entanglement generation due to gravitational interaction can be considered as evidence of the quantum nature of gravity [21, 22], which has sparked several investigations [23–36]. However, verifying the quantum nature of gravity requires entanglement between heavier objects [15, 18]. The realization of macroscopic quantum systems is pivotal for investigating the unexplored areas between the quantum world and gravity.

In this study, we consider the feasibility of realizing entanglement between macroscopic oscillators via optomechanical coupling. It is known that entanglement between two squeezed light beams with different squeezing angles is generated by passing them through the beam splitter. The authors of Ref. [37] analyzed the entanglement in a comparable situation where the power-recycled mirror squeezed the oscillators' common and differential modes differently. However, their analysis was limited to high-frequency regions, where the oscillators were regarded as free mass. Namely, they only demonstrated entanglement-generation between Fourier modes of macroscopic oscillator's motions in high-frequency regions. Therefore the previous work is not enough to include the analysis around resonant frequencies. Quantum control of macroscopic oscillators around resonant frequencies is important for entanglement-generation, e.g., Refs. [15, 18]. Then, our analysis here is not limited to high-frequency regions.

We revisit the realization of entanglement between macroscopic oscillators with the Kalman filter's formalism in a wide range of parameter spaces. We employ feedback control, which decreases the effective temperature, and detunes

---

\* miki.daisuke@phys.kyushu-u.ac.jp,  
nobuyuki.matsumoto@gakushuin.ac.jp,  
matsumura.akira@phys.kyushu-u.ac.jp,  
shichijo.tomoya@phys.kyushu-u.ac.jp,  
sugiyama.yuki@phys.kyushu-u.ac.jp,  
yamamoto@phys.kyushu-u.ac.jp,  
yamamoto@appi.keio.ac.jp

enabling us to trap the mechanical oscillator stably with the optical spring, as discussed in Ref. [6]. To clarify the difference between the previous [37] and present work, we note that the detuning was not considered in the previous work [37]. By using these quantum controls in an optomechanical system with a power-recycled mirror, we clarified the relationship between the entanglement and squeezing of states. Our results show that quantum cooperativity and detuning characterize the entanglement behavior, quantum squeezing, and purity. The entanglement generation requires quantum squeezing of both the common and differential modes of the oscillators. Squeezing, however, does not always result in entanglement generation, as high-purity squeezed states are also required. We demonstrate that the entanglement occurs for the quantum cooperativity  $C_{\pm}/n_{\text{th}}^{\pm} \gtrsim 3$  with the experimentally achievable parameters in amplitude quadrature measurement (X measurement).

The remainder of this paper is organized as follows: In Section II, we present a brief review of optomechanical systems while under continuous measurement and feedback control. In Section III, we provide a mathematical formula for the Riccati equation to describe the covariance matrix using a quantum Kalman filter to minimize the correlation. In Section IV, we extended the formulations in the previous sections to those with two optomechanical systems, in which we consider the entanglement between them through a beam splitter in a power-recycled interferometer. We determined the feasibility of preparing entanglements between the mirror oscillators in the space of the model parameter, depending on the amplitude quadrature measurement (X measurement) and phase quadrature measurement (Y measurement), respectively. Finally, Section V presents our conclusions. The derivation of the equations of motion for the system is presented in Appendix A. In Appendix B, we describe the details of logarithmic negativity for estimating the entanglement developed in this study. In Appendix C, we describe the details of computing the squeezing angle.

## II. FORMULAS

In this section, we consider a driven optical cavity mode that interacts with an oscillating mirror, which is regarded as a mechanical harmonic oscillator. The Hamiltonian of our system is as follows:

$$H = \frac{P^2}{2m} + \frac{1}{2}m\Omega^2 Q^2 + \hbar\omega_c a^\dagger a + \hbar\frac{\omega_c}{\ell} Q a^\dagger a + i\hbar E (a^\dagger e^{-i\omega_L t} - a e^{i\omega_L t}), \quad (1)$$

where  $Q$  and  $P$  are the canonical position and momentum operators of the oscillator, satisfying the commutation relation  $[Q, P] = i\hbar$ , while  $m$  and  $\Omega$  are the mass and resonance frequency of the oscillator, respectively;  $a$ ,  $a^\dagger$  are the annihilation and creation operators of the optical modes in the cavity,  $\ell$  is the cavity length, and  $\omega_c$  is the cavity frequency. The last term describes the input laser with frequency  $\omega_L$  and amplitude  $E = \sqrt{P_{\text{in}}\kappa/\hbar\omega_L}$ , where  $P_{\text{in}}$  is the input laser power and  $\kappa$  is the optical decay rate. Here, we introduce non-dimensional variables

$$q = \sqrt{\frac{2m\Omega}{\hbar}} Q, \quad p = \sqrt{\frac{2}{m\hbar\Omega}} P, \quad (2)$$

that satisfy the commutation relation  $[q, p] = 2i$ .

We consider the perturbation with respect to  $q \rightarrow \bar{q} + \delta q$ ,  $p \rightarrow \bar{p} + \delta p$ , and  $a' \rightarrow \bar{a}' + \delta a'$ , where  $a' = e^{i\omega_L t} a$  denotes the redefined annihilation operator. (See Appendix A-1 for more details). Note that  $(\bar{q}, \bar{p}, \bar{a}')$  are the expected values of  $(q, p, a')$ . By simply representing  $(\delta q, \delta p, \delta a')$  as  $(q, p, a')$ , we derive the following Langevin equation:

$$\dot{q} = \Omega p, \quad (3)$$

$$\dot{p} = -\Omega q - \Gamma p - 2g(e^{-i\phi} a' + e^{i\phi} a'^\dagger) + \sqrt{2\Gamma} p_{\text{in}} - \int_{-\infty}^t ds g_{FB}(t-s) X(s), \quad (4)$$

$$\dot{a}' = i\Delta a' - ig e^{i\phi} q - \frac{\kappa}{2} a' + \sqrt{\kappa} a_{\text{in}}, \quad (5)$$

where  $\bar{a}' = e^{i\phi} |\bar{a}'|$  and  $g = (|\bar{a}'| \omega_c / \ell) \sqrt{\hbar/2m\Omega}$  denote the optomechanical coupling.  $\Gamma$  and  $\Delta = \omega_L - \omega_c + 2g^2/\Omega$  denote the mechanical decay rate and detuning, respectively.  $p_{\text{in}}$  is the mechanical noise input with a variance of  $\langle p_{\text{in}}^2 \rangle = 2k_B T / \hbar\Omega + 1$ . Similarly,  $a_{\text{in}}$  is the optical noise input specified by  $\langle a_{\text{in}}^2 \rangle = (2N_{\text{th}} + 1)/2$  with thermal photon occupation number  $N_{\text{th}}$ . The last term in Eq. (4) describes the feedback effects and by introducing the amplitude quadrature  $x = e^{-i\phi} a' + e^{i\phi} a'^\dagger$  and the phase quadrature  $y = (e^{-i\phi} a' - e^{i\phi} a'^\dagger)/i$ , Eq. (5) yields

$$\dot{x} = -\frac{\kappa}{2} x - \Delta y + \sqrt{\kappa} x_{\text{in}}, \quad (6)$$

$$\dot{y} = -\frac{\kappa}{2} y + \Delta x + \sqrt{\kappa} y_{\text{in}} - 2gq, \quad (7)$$

where  $x_{\text{in}}$  and  $y_{\text{in}}$  are the corresponding input noises similarly defined as  $a_{\text{in}}$ , whose variance is specified by:  $\langle x_{\text{in}}^2 \rangle = \langle y_{\text{in}}^2 \rangle = 2N_{\text{th}} + 1$ .

Here, we consider the adiabatic limit  $\kappa \gg \Omega$ , which allows the continuous measurement of the oscillator position because the cavity photon dissipation is sufficiently larger than the frequency of the oscillator. In the limit of the dissipation domination  $\dot{x} = \dot{y} = 0$ , we have

$$x = \frac{8\Delta g}{\kappa^2 + 4\Delta^2}q + \frac{2\kappa\sqrt{\kappa}}{\kappa^2 + 4\Delta^2}x_{\text{in}} - \frac{4\Delta\sqrt{\kappa}}{\kappa^2 + 4\Delta^2}y_{\text{in}}, \quad (8)$$

$$y = -\frac{4\kappa g}{\kappa^2 + 4\Delta^2}q + \frac{4\Delta\sqrt{\kappa}}{\kappa^2 + 4\Delta^2}x_{\text{in}} + \frac{2\kappa\sqrt{\kappa}}{\kappa^2 + 4\Delta^2}y_{\text{in}}. \quad (9)$$

Introducing the rescaled variables

$$q = q' \sqrt{\frac{\Omega}{\omega_m}}, \quad p = p' \sqrt{\frac{\omega_m}{\Omega}}, \quad \omega_m = \sqrt{\Omega^2 + \Omega \frac{16\Delta g^2}{\kappa^2 + 4\Delta^2}}, \quad g_m = g \sqrt{\frac{\Omega}{\omega_m}}, \quad (10)$$

we rewrite the equation of motion as:

$$\dot{q}' = \omega_m p', \quad (11)$$

$$\dot{p}' = -\omega_m q' - \gamma_m p' + \sqrt{2\gamma_m} p'_{\text{in}} - \frac{4g_m \kappa \sqrt{\kappa}}{\kappa^2 + 4\Delta^2} x_{\text{in}} + \frac{8g_m \Delta \sqrt{\kappa}}{\kappa^2 + 4\Delta^2} y_{\text{in}}, \quad (12)$$

$$x = \frac{8\Delta g_m}{\kappa^2 + 4\Delta^2} q' + \frac{2\kappa\sqrt{\kappa}}{\kappa^2 + 4\Delta^2} x_{\text{in}} - \frac{4\Delta\sqrt{\kappa}}{\kappa^2 + 4\Delta^2} y_{\text{in}}, \quad (13)$$

$$y = -\frac{4\kappa g_m}{\kappa^2 + 4\Delta^2} q' + \frac{4\Delta\sqrt{\kappa}}{\kappa^2 + 4\Delta^2} x_{\text{in}} + \frac{2\kappa\sqrt{\kappa}}{\kappa^2 + 4\Delta^2} y_{\text{in}}, \quad (14)$$

where  $\gamma_m$  is the effective mechanical decay rate under feedback control, and the thermal noise input changes to  $\langle p'_{\text{in}}{}^2 \rangle = 2n_{\text{th}} + 1$  with  $n_{\text{th}} = k_B T \Gamma / \hbar \gamma_m \omega_m$ .

The quadratures of the optical cavity modes  $x$  and  $y$  contain information regarding the position of the mechanical oscillator  $q'$  in Eqs. (13) and (14). To estimate the oscillator position, we either consider the measurement of the amplitude quadrature  $x$ , or the measurement of the phase quadrature  $y$ . The observation signal of amplitude quadrature  $x$  is described by the following output equation:

$$X = \sqrt{\eta} x_{\text{out}} + \sqrt{1 - \eta} x'_{\text{in}}, \quad \text{with} \quad x_{\text{out}} = x_{\text{in}} - \sqrt{\kappa} x, \quad (15)$$

where  $\eta \in [0, 1]$  is the detection efficiency and  $x'_{\text{in}}$  is the additional vacuum noise for the imperfect measurement, which satisfies  $\langle x'_{\text{in}}{}^2 \rangle = 1$ . Under the limit of the dissipation domination, we have

$$X = -\frac{8g_m \Delta \sqrt{\eta \kappa}}{\kappa^2 + 4\Delta^2} q' - \sqrt{\eta} \frac{\kappa^2 - 4\Delta^2}{\kappa^2 + 4\Delta^2} x_{\text{in}} + \sqrt{\eta} \frac{4\kappa \Delta}{\kappa^2 + 4\Delta^2} y_{\text{in}} + \sqrt{1 - \eta} x'_{\text{in}}. \quad (16)$$

On the other hand, the observation signal of the phase quadrature  $y$  is also described by the output equation

$$Y = \sqrt{\eta} y_{\text{out}} + \sqrt{1 - \eta} y'_{\text{in}}, \quad \text{with} \quad y_{\text{out}} = y_{\text{in}} - \sqrt{\kappa} y, \quad (17)$$

which reduces to

$$Y = \frac{4g_m \kappa \sqrt{\eta \kappa}}{\kappa^2 + 4\Delta^2} q' - \sqrt{\eta} \frac{4\kappa \Delta}{\kappa^2 + 4\Delta^2} x_{\text{in}} - \sqrt{\eta} \frac{\kappa^2 - 4\Delta^2}{\kappa^2 + 4\Delta^2} y_{\text{in}} + \sqrt{1 - \eta} y'_{\text{in}}. \quad (18)$$

### III. RICCATI EQUATION

Because the observation signals in Eqs. (16) and (18) include noise information, we employed the quantum filter for optimal estimation. Here, we consider the quantum Kalman filter, which allows us to minimize the mean-squared error between the canonical operators  $\mathbf{r} = (q', p')^T$  and the estimated values  $\tilde{\mathbf{r}} = (\tilde{q}', \tilde{p})^T$ . i.e., each component of the covariance matrix  $\mathbf{V} = \langle \{\mathbf{r} - \tilde{\mathbf{r}}, (\mathbf{r} - \tilde{\mathbf{r}})^T\} \rangle$  is minimized. We rewrite the Langevin equation in matrix form as follows:

$$\frac{d}{dt} \mathbf{r} = \mathbf{A} \mathbf{r} + \begin{pmatrix} 0 \\ w \end{pmatrix}, \quad (19)$$

$$X = \mathbf{C}_X \mathbf{r} + v_X, \quad (20)$$

$$Y = \mathbf{C}_Y \mathbf{r} + v_Y, \quad (21)$$

where,

$$\mathbf{A} = \begin{pmatrix} 0 & \omega_m \\ -\omega_m & -\gamma_m \end{pmatrix}, \quad w = \sqrt{2\gamma_m} p'_{in} - \frac{4g_m \kappa^{3/2}}{\kappa^2 + 4\Delta^2} x_{in} + \frac{8g_m \kappa^{1/2} \Delta}{\kappa^2 + 4\Delta^2} y_{in}, \quad (22)$$

$$\mathbf{C}_X = \begin{pmatrix} -\frac{8g_m \Delta \sqrt{\kappa}}{\kappa^2 + 4\Delta^2} & 0 \\ 0 & 0 \end{pmatrix}, \quad v_X = -\frac{\kappa^2 - 4\Delta^2}{\kappa^2 + 4\Delta^2} \sqrt{\eta} x_{in} + \frac{4\kappa \Delta}{\kappa^2 + 4\Delta^2} \sqrt{\eta} y_{in} + \sqrt{1 - \eta} x'_{in}, \quad (23)$$

$$\mathbf{C}_Y = \begin{pmatrix} \frac{4g_m \kappa \sqrt{\eta \kappa}}{\kappa^2 + 4\Delta^2} & 0 \\ 0 & 0 \end{pmatrix}, \quad v_Y = -\frac{4\kappa \Delta}{\kappa^2 + 4\Delta^2} \sqrt{\eta} x_{in} - \frac{\kappa^2 - 4\Delta^2}{\kappa^2 + 4\Delta^2} \sqrt{\eta} y_{in} + \sqrt{1 - \eta} y'_{in}. \quad (24)$$

For the Kalman filter, we obtained the time evolution of the optimized covariance matrix as follows:

$$\frac{d\mathbf{V}}{dt} = \mathbf{A}\mathbf{V} + \mathbf{V}\mathbf{A}^T + \mathbf{N} - (\mathbf{V}\mathbf{C}_I^T + \mathbf{L}_I)\mathbf{M}^{-1}(\mathbf{V}\mathbf{C}_I^T + \mathbf{L}_I)^T, \quad (25)$$

where  $I = X$  or  $Y$ , and  $\mathbf{M} = \langle v_X^2 \rangle \mathbb{1}_2 = \langle v_Y^2 \rangle \mathbb{1}_2 = (2\eta N_{th} + 1) \mathbb{1}_2$  with  $2 \times 2$  identity matrix  $\mathbb{1}_2$ . Each matrix is given by

$$\mathbf{V} = \begin{pmatrix} V_{11} & V_{12} \\ V_{12} & V_{22} \end{pmatrix}, \quad \mathbf{N} = \begin{pmatrix} 0 & 0 \\ 0 & \langle w^2 \rangle \end{pmatrix}, \quad (26)$$

$$\mathbf{L}_X = \begin{pmatrix} 0 & 0 \\ \langle wv_X \rangle & 0 \end{pmatrix}, \quad \mathbf{L}_Y = \begin{pmatrix} 0 & 0 \\ \langle wv_Y \rangle & 0 \end{pmatrix}, \quad (27)$$

with

$$\langle w^2 \rangle = 2\gamma_m(2n_{th} + 1) + \frac{16g_m^2 \kappa}{\kappa^2 + 4\Delta^2} (2N_{th} + 1) \equiv \bar{n}, \quad (28)$$

$$\langle wv_X \rangle = \frac{4g_m \kappa \sqrt{\kappa \eta}}{\kappa^2 + 4\Delta^2} (2N_{th} + 1), \quad \langle wv_Y \rangle = \frac{8g_m \Delta \sqrt{\kappa \eta}}{\kappa^2 + 4\Delta^2} (2N_{th} + 1). \quad (29)$$

Considering the steady state  $\dot{\mathbf{V}} = 0$ , the covariance matrix satisfies the following equation:

$$\begin{aligned} 2\omega_m V_{12} - \lambda_I V_{11}^2 &= 0, \\ (\gamma_m + \lambda_I V_{11}) V_{12} + (V_{11} - V_{22}) \omega_m + \Lambda_I V_{11} &= 0, \\ 2\gamma_m V_{22} + 2\omega_m V_{12} + (\sqrt{\lambda_I} V_{12} + \Lambda_I / \sqrt{\lambda_I})^2 - \bar{n} &= 0, \end{aligned} \quad (30)$$

where we define

$$\lambda_X = \frac{64g_m^2 \eta \kappa \Delta^2}{(2\eta N_{th} + 1)(\kappa^2 + 4\Delta^2)^2}, \quad \lambda_Y = \frac{16g_m^2 \eta \kappa^3}{(2\eta N_{th} + 1)(\kappa^2 + 4\Delta^2)^2}, \quad (31)$$

$$\Lambda_X = -\Lambda_Y = -\frac{32g_m^2 \eta \kappa^2 \Delta}{(\kappa^2 + 4\Delta^2)^2} \frac{2N_{th} + 1}{2\eta N_{th} + 1}. \quad (32)$$

The solution of Eq. (30) is derived as follows:

$$\begin{aligned} V_{11} &= \frac{\gamma_I - \gamma_m}{\lambda_I}, \\ V_{12} &= \frac{(\gamma_I - \gamma_m)^2}{2\lambda_I \omega_m}, \\ V_{22} &= \frac{(\gamma_I - \gamma_m)(2\omega_m(\omega_m + \Lambda_I) + \gamma_I^2 - \gamma_m \gamma_I)}{2\lambda_I \omega_m^2}, \end{aligned} \quad (33)$$

where we defined

$$\gamma_I = \sqrt{\gamma_m^2 - 2\omega_m(\omega_m + \Lambda_I) + 2\omega_m \sqrt{\omega_m(\omega_m + 2\Lambda_I) + \bar{n}\lambda_I}}. \quad (34)$$

The covariance matrix in Eqs. (33) is also derived using the Wiener filter for the steady state, and is consistent with Ref. [6] in relation to the  $X$  measurement. The results for the  $Y$  measurement with  $\Delta = 0$ ,  $N_{th} = 0$ , and with no feedback control is consistent with that reported in Ref. [7].

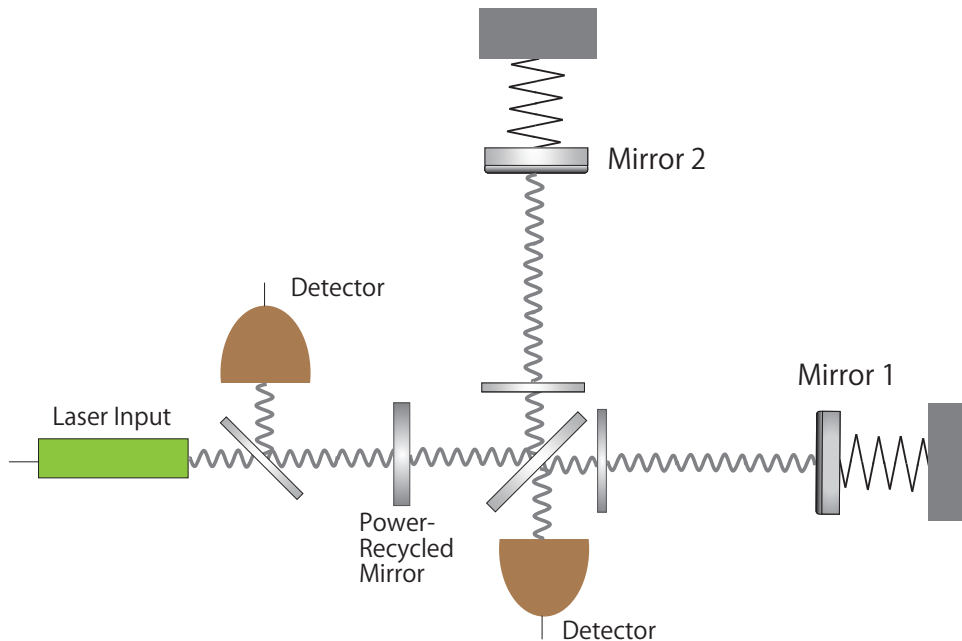


FIG. 1: Schematic representation of Power-Recycled-Fabry-Perot-Michelson interferometer.

#### IV. ENTANGLEMENT BETWEEN TWO MIRRORS

Here, we consider the entanglement between two oscillators coupled with optical modes and passing through the beam splitter in a power-recycled-Fabry-Perot-Michelson interferometer. Fig. 1 shows a schematic plot of this configuration. In quantum optics, passing two squeezed beams through a beam splitter becomes entangled when the squeezing angles are different. Ref. [37] shows that the entanglement between two oscillators where coupled cavity modes occur by passing the output beams through the beam splitter. However, the  $Y$  measurement is only considered in the high-frequency region, where the oscillator can be considered as a free mass. In this study, however, our general analysis of the entanglement behavior is not limited to the free-mass region. This is achieved through detuning and feedback effects for  $X$  and  $Y$  measurements, respectively.

Here, we assumed that the individual background quadratures were equal to  $\bar{q}_1 = \bar{q}_2$ ,  $\bar{p}_1 = \bar{p}_2$ , and  $\bar{a}_1 = \bar{a}_2$ , and the background is in a steady state  $\dot{\bar{q}} = \dot{\bar{p}} = \dot{\bar{a}} = 0$ . By introducing the quadratures of the common and differential modes as  $q_{\pm} = (q_1 \pm q_2)/\sqrt{2}$ ,  $p_{\pm} = (p_1 \pm p_2)/\sqrt{2}$ , and  $a_{\pm} = (a_1 \pm a_2)/\sqrt{2}$ , we derive the background equations as:

$$\begin{aligned} \bar{q}_+ &= -\frac{\sqrt{2}G|\bar{a}_+|^2}{\Omega}, & \bar{q}_- &= 0, \\ \bar{p}_{\pm} &= 0, \\ \bar{a}_+ &= \frac{2E_+}{\kappa_+ - 2i\Delta}, & \bar{a}_- &= 0, \end{aligned} \quad (35)$$

and the perturbation equations are as follows:

$$\begin{aligned} \dot{q}_{\pm} &= \Omega p_{\pm}, \\ \dot{p}_{\pm} &= -\Omega q_{\pm} - 2g(e^{-i\phi}a_{\pm} + e^{i\phi}a_{\pm}^{\dagger}) - \Gamma p_{\pm} + \sqrt{2}\Gamma p_{\text{in}}^{\pm}, \\ \dot{a}_{\pm} &= i\Delta a_{\pm} - ig e^{i\phi} q_{\pm} - \frac{\kappa_{\pm}}{2} a_{\pm} + \sqrt{\kappa_{\pm}} a_{\text{in}}^{\pm}, \end{aligned} \quad (36)$$

where  $E_+ = \sqrt{P_{\text{in}}\kappa_+/\hbar\omega_L}$  denotes the input-laser amplitude in the common cavity.  $\Delta = \omega_L - \omega_c + 2g^2/\Omega$  represents detuning, and we defined  $g = |\bar{a}_+|G/\sqrt{2}$  with  $G = (\omega_c/\ell)\sqrt{\hbar/2m\Omega}$ , as represented in the previous section on optomechanical coupling. The derivation of these equations is presented in Appendix A-2. The asymmetry between the common and differential modes originates from Power-recycling mirrors in the common mode, which is described

| Symbol  | Name  | Value                               |
|---|---|-------------------------------------|
| $\Omega$  | Mechanical frequency  | $2\pi \times 2.2$ Hz                |
| $\Gamma(\Omega)$                                    | Mechanical decay rate   | $2\pi \times 10^{-6}$ Hz            |
| $\gamma_m$  | Effective mechanical decay rate under feedback control        | $2\pi \times 6.9 \times 10^{-3}$ Hz |
| $T$   | Bath temperature  | 300 K                               |
| $\delta_- = \Delta/\kappa_-$                        | (Normalized) detuning   | 0.2                                 |
| $\zeta$   | Normalized detuning ratio of differential mode to common mode | 3                                   |
| $\eta$  | Detection efficiency  | 0.92                                |
| $N_{\text{th}}$                                     | Thermal photon number   | 0                                   |
| $Q_- = \omega_m^-/\gamma_m$                         | Quality factor  | $7.5 \times 10^4$                   |
| $Q_+$ is defined by Eq. (52)                        |   | $1.6 \times 10^5$                   |
| $C_- = 4(g_m^-)^2/\gamma_m\kappa_-$                 | Cooperativity   | $1.1 \times 10^5$                   |
| $C_+$ is defined by Eq. (53)                        |   | $1.6 \times 10^5$                   |
| $n_{\text{th}}^-$                                   | Thermal phonon number   | $7.5 \times 10^3$                   |
| $n_{\text{th}}^+$ is defined by Eq. (54)            |   | $1.8 \times 10^3$                   |
| $m$   | Mirror mass   | $7.71 \times 10^{-6}$ kg            |
| $\ell$  | Cavity length   | $10^{-1}$ m                         |
| $\omega_L$  | Laser frequency   | $2\pi \times 300 \times 10^{12}$ Hz |
| $\kappa_-$  | Optical decay rate  | $2\pi \times 1.64 \times 10^6$ Hz   |
| $ \bar{a} $   | Expectation value of cavity photon quadrature                 | $1.27 \times 10^5$                  |
| $g =  \bar{a} (\omega_c/\ell)\sqrt{\hbar/2m\Omega}$ | Optomechanical coupling                                       | $1.69 \times 10^6$ Hz               |
| $F = 2\pi c/\ell\kappa_-$                           | Finesse   | $1.8 \times 10^3$                   |
| $P_{\text{in}}$                                     | Input laser power   | 30 mW                               |

**TABLE I:** Parameters adopted as a feasible tabletop experiment expected from the state-of-art technique [5, 6]. The detuning for the common mode is  $\delta_+ = \zeta\delta_-$ , and  $Q_+$ ,  $C_+$ , and  $n_{\text{th}}^+$  are decided in Eqs. (52)-(54).

by the difference in optical decay rates for each mode  $\kappa_{\pm}$ . The optical decay rates for the differential mode  $\kappa_-$  and common mode  $\kappa_+$  are introduced in their Langevin equations and the power-recycled mirror makes the optical decay rate of the common mode smaller than that of the differential mode by reflecting only a portion of the common-mode light. Here, we introduce the parameter  $\zeta \geq 1$  to describe the asymmetry using

$$\kappa_+ = \frac{1}{\zeta}\kappa_-. \quad (37)$$

Therefore, in our framework,  $\zeta$  describes the asymmetry between common and differential modes, which causes entanglement owing to the half-beam splitter.

Using the procedure described in Sec. II and Sec. III, we obtain the components of the covariance matrices for the common and differential modes  $\mathbf{V}_{\pm}$  (see Eq. (46)) as follows :

$$\begin{aligned} V_{11}^{\pm} &= \frac{\gamma_I^{\pm} - \gamma_m}{\lambda_I^{\pm}}, \\ V_{12}^{\pm} &= \frac{(\gamma_I^{\pm} - \gamma_m)^2}{2\lambda_I^{\pm}\omega_m^{\pm}}, \\ V_{22}^{\pm} &= \frac{(\gamma_I^{\pm} - \gamma_m)(2\omega_m^{\pm}(\omega_m^{\pm} + \Lambda_I^{\pm}) + (\gamma_I^{\pm})^2 - \gamma_m\gamma_I^{\pm})}{2\lambda_I^{\pm}(\omega_m^{\pm})^2}, \end{aligned} \quad (38)$$

where,

$$\omega_m^\pm = \sqrt{\Omega^2 + \Omega \frac{16\Delta g^2}{\kappa_\pm^2 + 4\Delta^2}}, \quad g_m^\pm = g \sqrt{\frac{\Omega}{\omega_m^\pm}}, \quad (39)$$

$$\lambda_X^\pm = \frac{64(g_m^\pm)^2 \kappa_\pm \Delta^2 \eta}{(2\eta N_{\text{th}} + 1)(\kappa_\pm^2 + 4\Delta^2)^2}, \quad \lambda_Y^\pm = \frac{16(g_m^\pm)^2 \kappa_\pm^3 \eta}{(2\eta N_{\text{th}} + 1)(\kappa_\pm^2 + 4\Delta^2)^2}, \quad (40)$$

$$\Lambda_X^\pm = -\Lambda_Y^\pm = -\frac{32(g_m^\pm)^2 \kappa_\pm^2 \Delta \eta}{(\kappa_\pm^2 + 4\Delta^2)^2} \frac{2N_{\text{th}} + 1}{2\eta N_{\text{th}} + 1}, \quad (41)$$

$$\bar{n}_\pm = 2\gamma_m(2n_{\text{th}}^\pm + 1) + \frac{16(g_m^\pm)^2 \kappa_\pm}{\kappa_\pm^2 + 4\Delta^2} (2N_{\text{th}} + 1), \quad n_{\text{th}}^\pm = \frac{k_B T \Gamma}{\hbar \gamma_m \omega_m^\pm}, \quad (42)$$

$$\gamma_I^\pm = \sqrt{\gamma_m^2 - 2\omega_m^\pm(\omega_m^\pm + \Lambda_I^\pm) + 2\omega_m^\pm \sqrt{\omega_m^\pm(\omega_m^\pm + 2\Lambda_I^\pm) + \bar{n}_\pm \lambda_I^\pm}}. \quad (43)$$

Then, we obtain the solution for each oscillator's canonical operator with a transformation operation using the half-beam splitter:

$$\begin{pmatrix} \mathcal{Q}_1 \\ \mathcal{P}_1 \\ \mathcal{Q}_2 \\ \mathcal{P}_2 \end{pmatrix} = \mathbf{S} \begin{pmatrix} \mathcal{Q}_+ \\ \mathcal{P}_+ \\ \mathcal{Q}_- \\ \mathcal{P}_- \end{pmatrix}, \quad \mathbf{S} = \frac{1}{\sqrt{2}} \begin{pmatrix} 1 & 0 & 1 & 0 \\ 0 & 1 & 0 & 1 \\ 1 & 0 & -1 & 0 \\ 0 & 1 & 0 & -1 \end{pmatrix}, \quad (44)$$

where  $\mathcal{Q}_\pm = \sqrt{\hbar/2m\omega_m^\pm} q_\pm$ ,  $\mathcal{P}_\pm = \sqrt{\hbar m \omega_m^\pm/2} p_\pm$  are the dimensional operators satisfying  $[\mathcal{Q}_\pm, \mathcal{P}_\pm] = i\hbar$ . The covariance matrix with the basis of each oscillator  $(\mathcal{Q}_1, \mathcal{P}_1, \mathcal{Q}_2, \mathcal{P}_2)$  is given by

$$\mathbf{V}' = \mathbf{S} \begin{pmatrix} \mathbf{V}_+ & 0 \\ 0 & \mathbf{V}_- \end{pmatrix} \mathbf{S} \equiv \begin{pmatrix} \mathbf{V}_1 & \mathbf{V}_{12} \\ \mathbf{V}_{12} & \mathbf{V}_2 \end{pmatrix}, \quad (45)$$

where  $\mathbf{V}_\pm$  is defined as:

$$\mathbf{V}_\pm = \begin{pmatrix} V_{\mathcal{Q}\mathcal{Q}}^\pm & V_{\mathcal{Q}\mathcal{P}}^\pm \\ V_{\mathcal{P}\mathcal{Q}}^\pm & V_{\mathcal{P}\mathcal{P}}^\pm \end{pmatrix}, \quad (46)$$

and  $\mathbf{V}_1$ ,  $\mathbf{V}_{12}$ , and  $\mathbf{V}_2$  are  $2 \times 2$ -component matrices defined by Eq. (45). To analyze the entanglement behavior, we introduce logarithmic negativity as:

$$E_N = \max \left\{ 0, -\log_2 \left( \frac{2}{\hbar} \sqrt{\frac{\Sigma - \sqrt{\Sigma^2 - 4\det \mathbf{V}'}}{2}} \right) \right\}, \quad (47)$$

where  $\Sigma = \det \mathbf{V}_1 + \det \mathbf{V}_2 - 2\det \mathbf{V}_{12}$ . For a two-mode Gaussian state, the system is only entangled if the logarithmic negativity is positive  $E_N > 0$ . The critical value  $\epsilon_{\text{cr}}$  is defined as the second part of the brace in Eq. (47),

$$\epsilon_{\text{cr}} = -\log_2 \left( \frac{2}{\hbar} \sqrt{\frac{\Sigma - \sqrt{\Sigma^2 - 4\det \mathbf{V}'}}{2}} \right) \quad (48)$$

and  $\epsilon_{\text{cr}} > 0$  shows that the state is entangled. Using the steady-state covariance matrix for the common and differential modes, we have

$$\Sigma = \frac{\hbar^2(\gamma_+ - \gamma_m)(\gamma_- - \gamma_m)}{8\lambda_I^+ \lambda_I^-} \left( \frac{\gamma_+^2 + \gamma_-^2 - \gamma_+ \gamma_- - \gamma_m^2}{\omega_m^+ \omega_m^-} + 2 \frac{\Lambda_I^+ + \omega_m^+}{\omega_m^-} + 2 \frac{\Lambda_I^- + \omega_m^-}{\omega_m^+} \right), \quad (49)$$

$$\det \mathbf{V}' = \left( \frac{\hbar^2(\gamma_+ - \gamma_m)(\gamma_- - \gamma_m)}{16\lambda_I^+ \lambda_I^-} \right)^2 \left( \frac{\gamma_+^2 - \gamma_m^2}{(\omega_m^+)^2} + 4 \frac{\Lambda_I^+}{\omega_m^+} + 4 \right) \left( \frac{\gamma_-^2 - \gamma_m^2}{(\omega_m^-)^2} + 4 \frac{\Lambda_I^-}{\omega_m^-} + 4 \right). \quad (50)$$

We introduce the quality factor  $Q_{\pm}$  and cooperativity  $C_{\pm}$  as:

$$Q_{\pm} = \frac{\omega_m^{\pm}}{\gamma_m}, \quad C_{\pm} = \frac{4(g_m^{\pm})^2}{\gamma_m \kappa_{\pm}}. \quad (51)$$

We can derive logarithmic negativity as a function of  $Q_{\pm}$ ,  $C_{\pm}$ ,  $n_{\text{th}}^{\pm}$ ,  $N_{\text{th}}$ ,  $\Delta/\kappa_{\pm}$ , and  $\eta$  (see Appendix B). Additionally, our results are not limited to the free-mass region. By introducing the normalized detuning  $\delta_{\pm} = \Delta/\kappa_{\pm}$ , the relation (37) leads to:

$$Q_+ = Q_- \left( 1 + \frac{4C_- \delta_- (\zeta^2 - 1)}{Q_- (1 + 4\delta_-^2)(1 + 4\zeta^2 \delta_-^2)} \right)^{1/2}, \quad (52)$$

$$C_+ = \zeta C_- \left( 1 + \frac{4C_- \delta_- (\zeta^2 - 1)}{Q_- (1 + 4\delta_-^2)(1 + 4\zeta^2 \delta_-^2)} \right)^{-1/2}. \quad (53)$$

Whereas the resonance frequency is written as  $\Omega/\gamma_m = \sqrt{Q(Q - 4C\delta + 4Q\delta^2)/(1 + 4\delta^2)}$ , the stability condition  $Q_{\pm}(1 + 4\delta_{\pm}^2) > 4C_{\pm}\delta_{\pm}$  is always satisfied for  $\delta_{\pm} > 0$  from the definition (51). As a result, we note that the stability condition is satisfied for any  $(C_{\pm}, Q_{\pm}, \delta_{\pm})$  as long as  $\delta_{\pm} > 0$ .

Next, we discuss the entanglement behavior of our results. We adopt the parameters in Table I, some of which have already been achieved [5, 6], whereas others are conservative parameters expected in the mid-term future. Here we

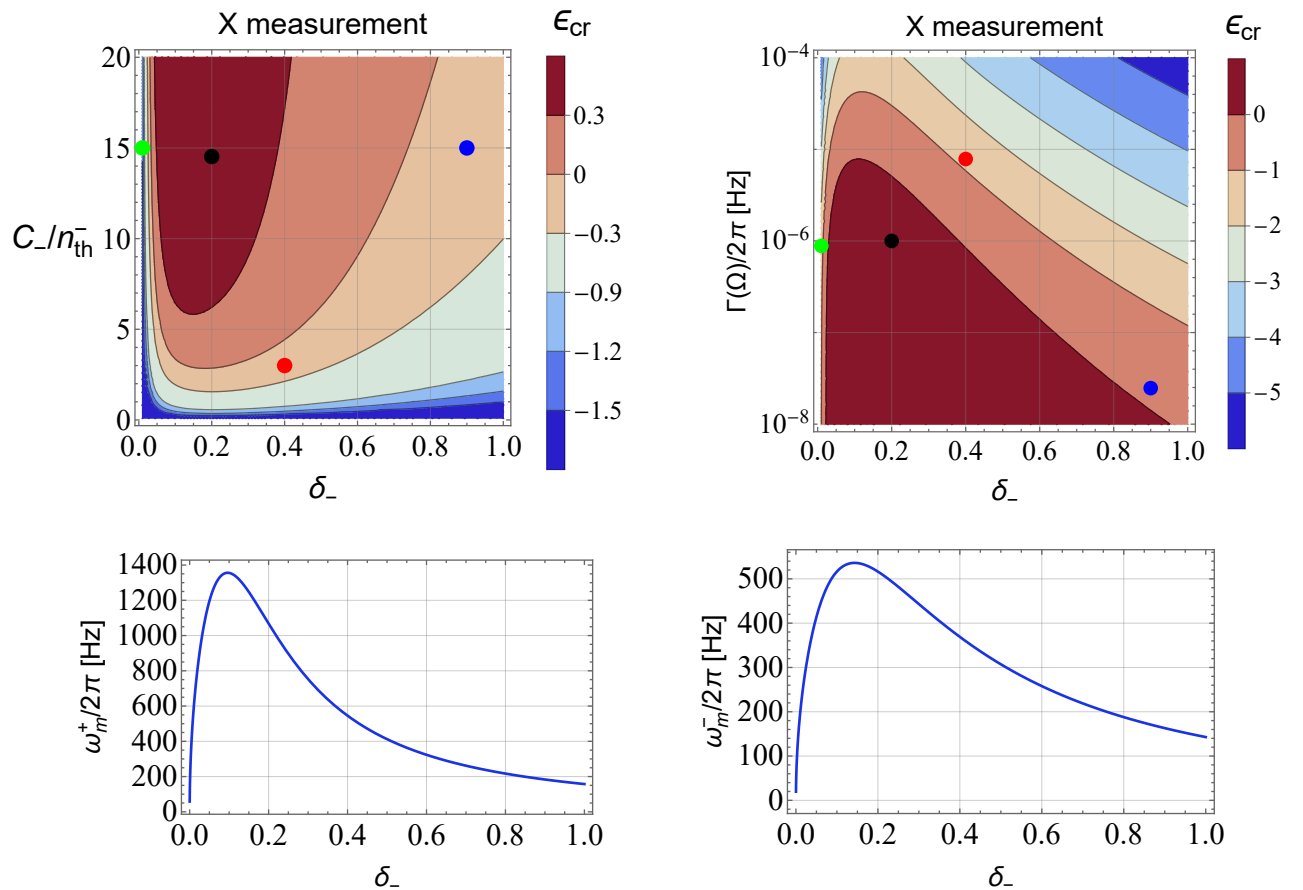


**FIG. 2:** Upper panels: The critical value  $\epsilon_{\text{cr}}$  as a function of  $C_-/n_{\text{th}}^-$  and  $\delta_-$  for the  $X$  measurement is shown in the upper left panel, while the same is shown as a function of  $\Gamma(\Omega)/2\pi$  and  $\delta_-$  in the upper right panel. Here we assumed the structural damping  $\Gamma(\omega_m^{\pm}) = \Gamma(\Omega)\Omega/\omega_m^{\pm}$ , which leads to  $n_{\text{th}}^{\pm} = k_B T \Gamma(\Omega)\Omega/\hbar\Gamma_m(\omega_m^{\pm})^2$ . We also assumed that the environmental temperature  $T$ , effective mechanical frequency  $\Omega$ , and optical decay rate  $\kappa_{\pm}$  are fixed, which are given in Table I. The entanglement generation between two oscillators is achieved for the region in brown and in dark brown  $\epsilon_{\text{cr}} > 0$  in the left panel, and for region in dark brown in the right panel, including black circle. We also show the entanglement behavior of each point as a function  $\zeta$  in Figure 9 with the same color curve. Lower panels: The lower left and right panels show  $\omega_m^+$  and  $\omega_m^-$  as functions of  $\delta_-$ , respectively.



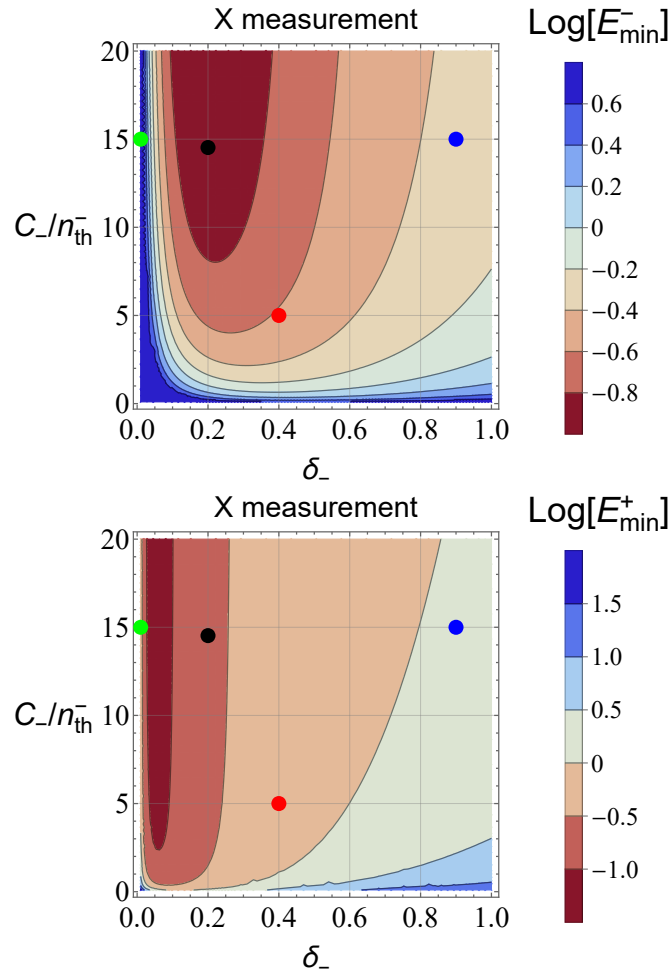


**FIG. 3:** The logarithm of the minimum eigenvalue for the differential mode covariance matrix  $E_{\min}^-$  is shown in the upper panel, while the same operation for the common mode  $E_{\min}^+$  is shown in the lower panel.

assume the structural damping  $\Gamma(\omega_m^\pm) = \Gamma(\Omega)\Omega/\omega_m^\pm$ , which leads to

$$n_{\text{th}}^\pm = \frac{k_B T \Gamma(\Omega) \Omega}{\hbar \gamma_m (\omega_m^\pm)^2}. \quad (54)$$

We now consider the tabletop experiments with mg scale mirrors, so assume that the mechanical frequency  $\Omega$ , effective mechanical decay rate  $\gamma_m$ , bath temperature  $T$ , optical decay rate  $\kappa_\pm$ , and ratio of the optical decay rate  $\zeta$  are fixed as those in Table I; the variable parameters are the bare mechanical decay rate  $\Gamma$  and the detuning  $\Delta$ . The upper left panel of Figure 2 plots  $\epsilon_{\text{cr}}$  for the X measurement as a function of the quantum cooperativity  $C_-/n_{\text{th}}^-$  and the normalized detuning  $\delta_-$ . Here, the quantum cooperativity depends on both  $\Gamma$  and  $\delta_\pm$ , and the upper right panel of Fig. 2 shows the same plot as a function of  $\Gamma$  and  $\delta_-$ . Entanglement appears for  $\epsilon_{\text{cr}} > 0$ , which is achieved for the brown and dark brown regions in the upper left panel, and for the dark brown region in the upper right panel, including the black circle. The minimum quantum cooperativity required to generate the entanglement is  $C_-/n_{\text{th}}^- \simeq 3$ , and  $\delta_- \simeq 0.1 \sim 0.2$  is advantageous in generating entanglement for the X measurement. The lower panels of Fig. 2 show the behavior of the frequency  $\omega_m^\pm$  as a function of the detuning  $\delta_-$ . In the X measurement, the entanglement is optimized near the peak of the frequency of both modes,  $800[\text{Hz}] \lesssim \omega_m^+/2\pi \lesssim 1.4[\text{kHz}]$  and  $400[\text{Hz}] \lesssim \omega_m^-/2\pi \lesssim 500[\text{Hz}]$ .

Figure 3 shows the logarithm of the minimum eigenvalue for the covariance matrix, for X measurement as a function of  $C_-/n_{\text{th}}^-$  and  $\delta_-$ . When the minimum eigenvalue is less than 1, the state is quantum-squeezed because the squeezed uncertainty is less than that of the vacuum state. Therefore, the region,  $C_-/n_{\text{th}}^- \gtrsim 1$  and  $0.1 \lesssim \delta_- \lesssim 0.8$  roughly, satisfies the condition of a quantum-squeezed state.

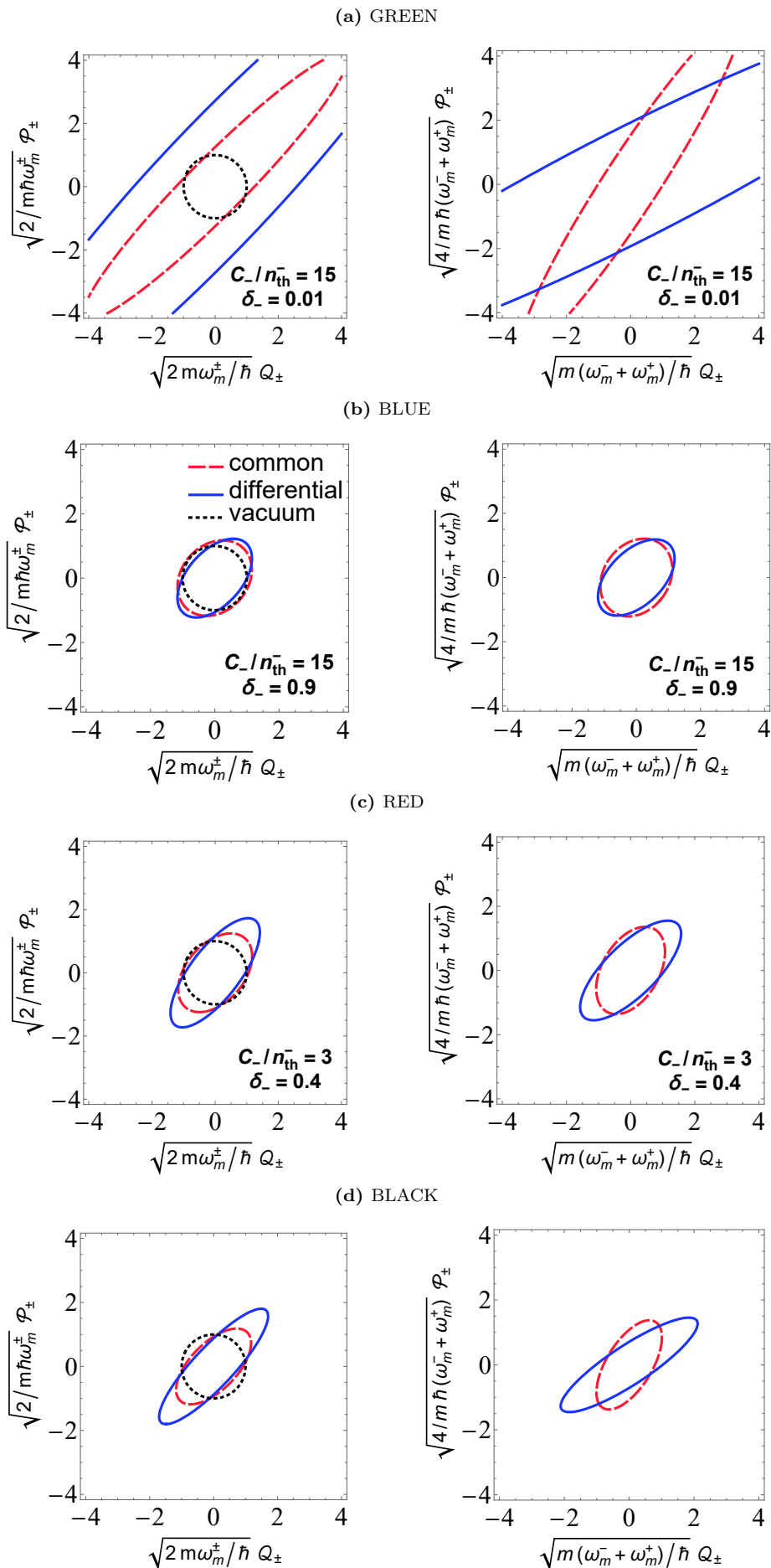


**FIG. 4:** The Wigner ellipses of the common mode (red dashed line), differential mode (blue solid line), and ground state (black dotted line). The covariance matrices of common and differential modes are normalized with the frequency  $\omega_m^\pm$  in the left panels and with  $(\omega_m^+ + \omega_m^-)/2$  in the right panels. Each panel corresponds to the parameters specified by the colored circle in Fig. 2, (a) is the green circle, (b) is the white circle, (c) is the blue circle, and (d) is the black circle. The circles with the same color in Figs. 2, 3, 5, 6, and 7 assume the same parameters.

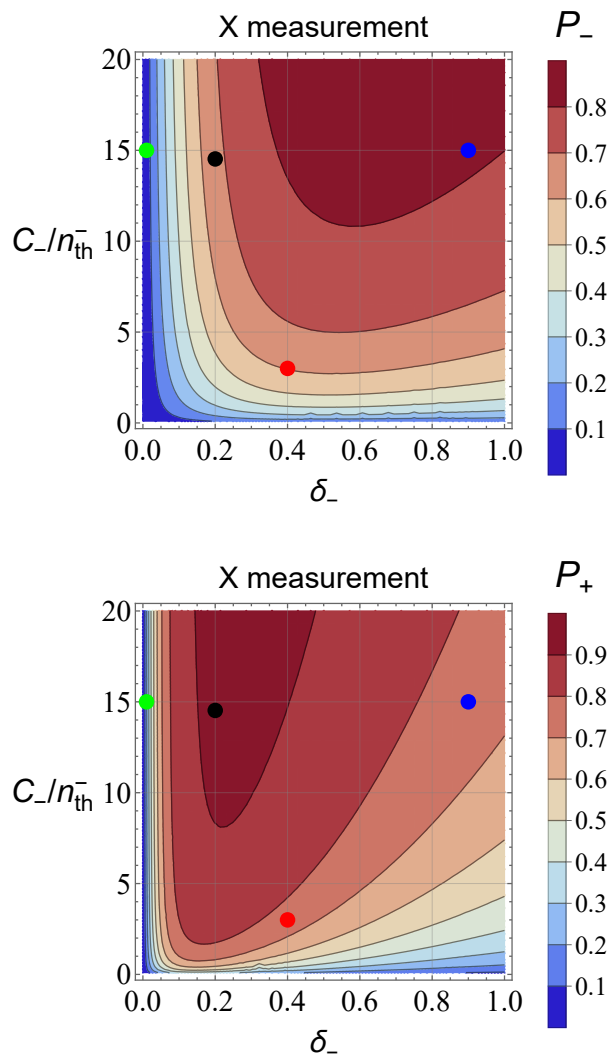


**FIG. 5:** The behavior of the purity of differential (upper panel) and common (lower panel) modes.

The red dashed, blue solid, and black dotted curves in Fig. 4 show the ellipses obtained when the Wigner functions  $W$  of the common mode, the differential mode, and the ground state satisfy  $W = e^{-1}W_{\max}$ , respectively. Each panel assumes that the parameters  $C_-/n_{\text{th}}^-$  and  $\delta_-$  correspond to the colored circles in Figs. 2 and 3, respectively. Panel (a) in Fig. 4, which correspond to the green circle in Figs. 2 and 3, respectively, show the case when neither mode is quantum-squeezed and the entanglement does not occur. Panel (b) and (c), corresponding to the white and blue circles, illustrate the case in which only differential modes, and both the common and differential modes are quantum-squeezed, respectively. However, the entanglement is not generated in the case for the panel (b) and (c). Panel (d), corresponding to the black circle represents an experimentally feasible parameter expected from the proposed technique [5, 6] by using  $C_{\pm}$ ,  $n_{\text{th}}^{\pm}$ , and  $Q_{\pm}$  in Table I. In this case, both the modes are quantum-squeezed and the entanglement is generated.

Now we discuss the relationship between quantum squeezing and entanglement. The blue circle in the upper panels of Figs. 2 and 3 demonstrates that squeezing does not necessarily imply the generation of entanglement. As shown in panel (c) of Fig. 4, where entanglement is not generated in Fig. 2, we find that the differential and common modes are in a quantum-squeezed state. We infer that purity plays a role in the generation of entanglement. Figure 5 plots the purity as a function of  $C_-/n_{\text{th}}^-$  and  $\delta_-$  for the differential mode (upper panel) and common mode (lower panel). We find that the high purity and the quantum-squeezing are necessary for generating entanglement.

Figure 6 plots the difference of squeezing angle between the common mode and the differential mode as a function of  $C_-/n_{\text{th}}^-$  and  $\delta_-$ , where squeezing angle is defined using the Wigner ellipses normalized with the  $\omega_m^{\pm}$  as shown in the left panels of Fig. 4. One can see that the difference of the squeezing angle is quite small in the entire region of the plot. From an analogy of the entanglement generation by passing the two squeezed beams through an half

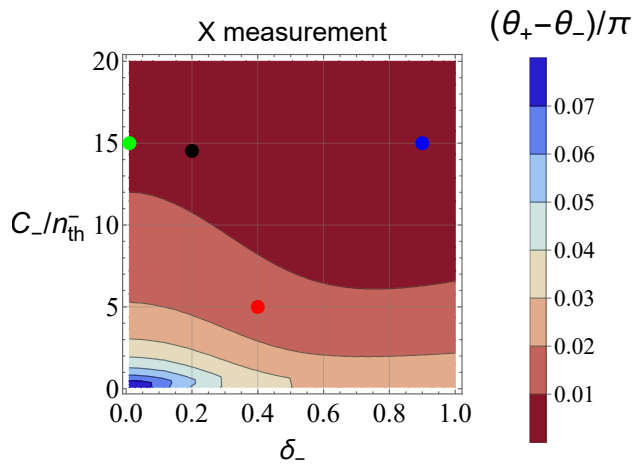


**FIG. 6:** The behavior of the difference of two squeezing angles between common mode and differential mode normalized by the frequency  $\omega_m^\pm$ , which is small in our system.

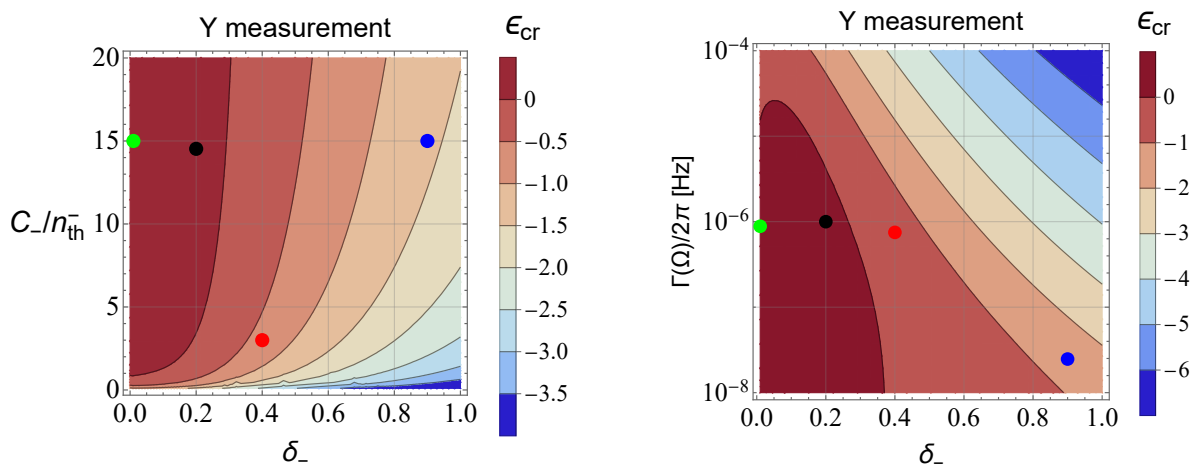


**FIG. 7:** Same as the upper panels of Fig. 2 but for the Y measurement.

beam splitter, it is known that the difference in the squeezing angles is an important factor. However, the result of Fig. 6 shows that the entanglement can be generated even for the cases of the small difference of squeezing angle between the common mode and the differential mode. One can understand that the difference of the amplitude of the squeezing plays a role for the entanglement generation. This might be rephrased that the entanglement generation occurs when the squeezing angles of the Wigner ellipses when normalized by the common frequency  $(\omega_m^+ + \omega_m^-)/2$  are quite different, as shown in the right panels of Fig. 4. We note that these differences of the normalization do not affect the entanglement at all because the entanglement does not depend on the normalization of the Wigner ellipse.

We next discuss the entanglement behavior and phase distribution for the Y measurement in Figs. 7 and 8, which are similar to those of the X measurement. Figure 7 shows that the entanglement is more easily generated for small  $\delta_\pm$  compared to the case in the X measurement (upper panels of Fig. 2). The difference is understood by the efficiency of the measurements, which is described by the first term of the right hand side of Eqs. (16) and (18). The ellipses in Fig. 8 show the significance of squeezing for the Y measurement, where each panel corresponds to the parameters specified by the colored circles in Fig. 7. For the free-mass limit with  $\delta_\pm = 0$  and  $\zeta \sim 70$ , the squeezing angles look near orthogonal when the Wigner ellipses are normalized by the common measurement rate, which is consistent with Ref. [37]. From an experimental point of view, it should be noted that conducting the homodyne (Y) measurement assumed in the Table I is not easy due to the problem of detection of such a high-power laser, which might make entanglement generation with the X measurement advantageous under the condition of the parameters in Table I. Finesse can be enhanced in order to avoid this difficulty; however, it reduces the linear range of the optical cavity such that cavity length control becomes difficult.

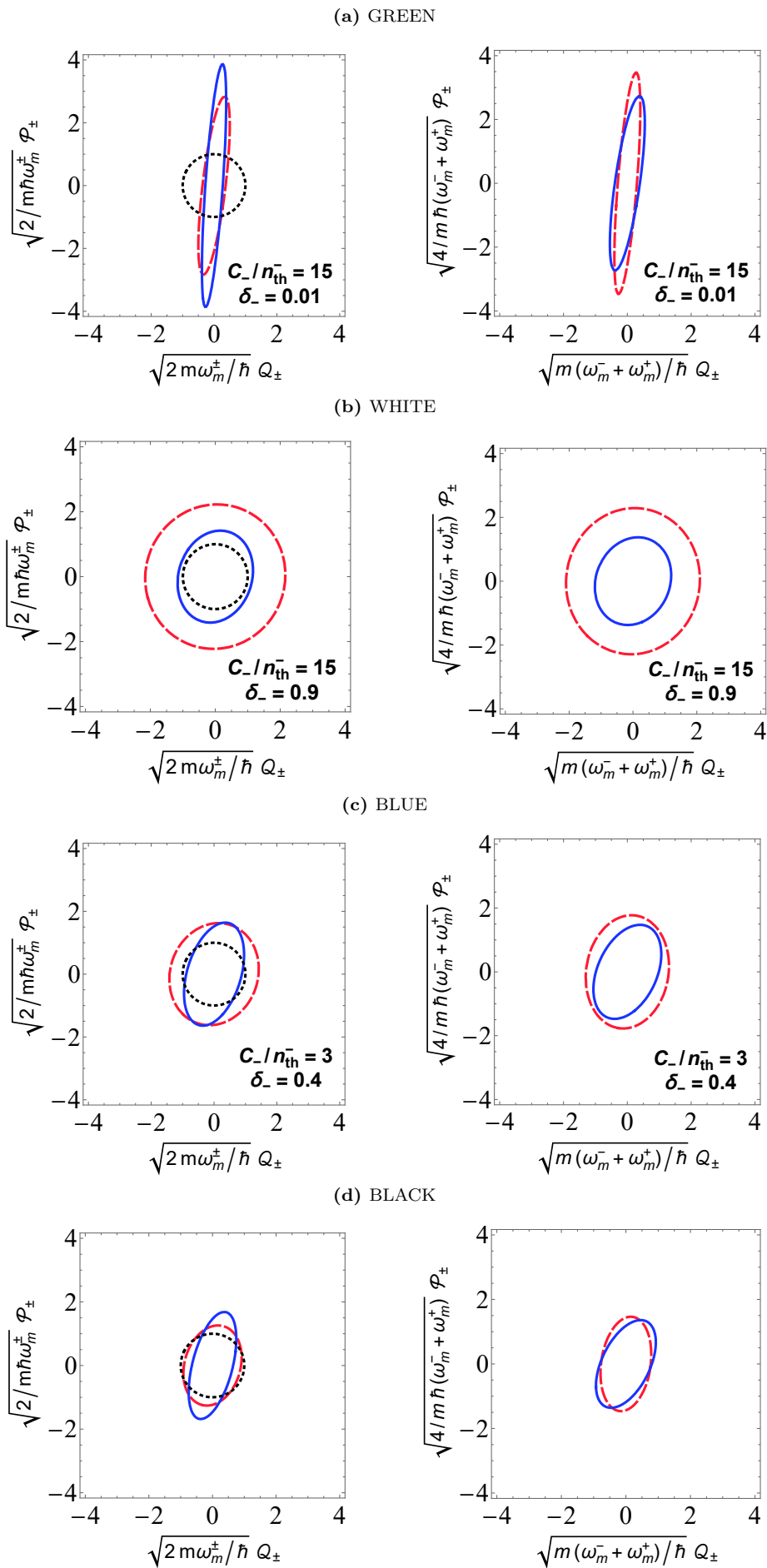


**FIG. 8:** Same as Fig. 4 but for the Y measurement, i.e., the Wigner ellipses in the the phase space for the colored grid points in Fig. 7.

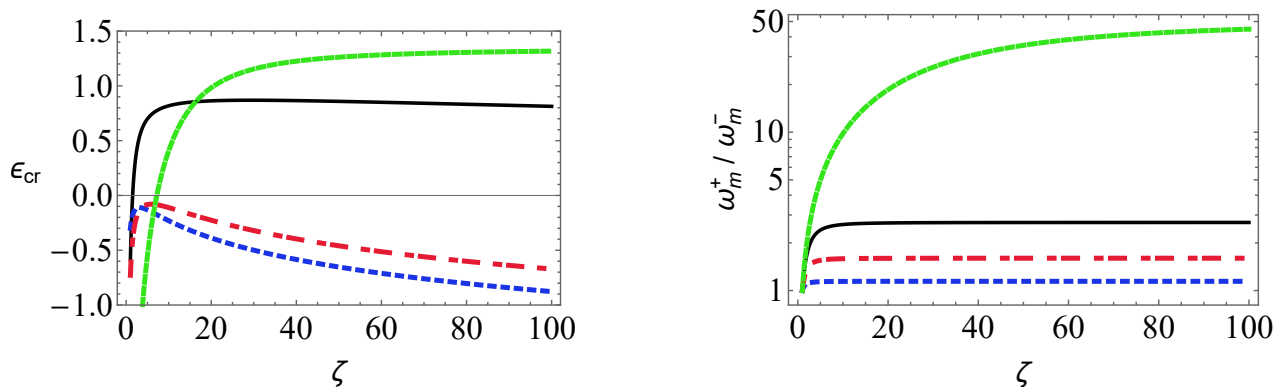


**FIG. 9:** The behavior of the logarithmic negativity for the X measurement (left panel) and the ratio of frequency of the common mode to that of the differential mode (right panel) as a function of  $\zeta$ . Each curve in the four colors assumes the same parameters as those of the circle in the same corresponding color in Fig. 2.

In the above analysis we fixed the parameter  $\zeta = 3$ , which characterizes the asymmetry of the common and differential modes. Here we discuss how the entanglement behavior depends on the parameter  $\zeta$ . Figure 9 shows the logarithmic negativity for the X measurement (left panel) and the frequency ratio  $\omega_m^+/\omega_m^-$  (right panel) as a function of  $\zeta$ . The entanglement with the parameters in Table I, which is the solid black curve, saturates for  $\zeta \gtrsim 10$ . The green curve increases significantly as  $\zeta$  increases. To understand the behaviors of this figure, we infer that the joint effect of the common mode and the differential mode on the entanglement is important. Even when the purity of the differential mode is small, the entanglement appears by increasing the purity of the common mode when  $\zeta$  increases. Furthermore, the measurement efficiency, which is the coefficient of  $q$  in the first term of the right hand side in Eq. (16), plays an important role for the squeezing through the detuning parameter when  $\zeta$  changes. Thus  $\zeta$  is important for entanglement to control the purity and the asymmetry of the squeezing between the common and the differential modes which is caused by the asymmetric measurement efficiency.

## V. SUMMARY AND CONCLUSIONS

We investigated the feasibility of generating a macroscopic entanglement between mechanical oscillators coupled with cavity optical modes under continuous measurement and feedback control. The mechanical oscillators are trapped with an optical spring owing to the detuning and squeezing achieved by measuring the output light. We considered a Fabry–Perot–Michelson interferometer with a power-recycled mirror to generate asymmetry between the common and differential modes. In this system, the two oscillators are entangled by the optical beams passing through the half-beam splitter. This follows from the fact that the entangled beam is generated by squeezed beams passing through a half-beam splitter. In our optomechanical systems, the squeezed states of optical beams are produced through measurement with the Kalman filter, which optimizes the estimation of the oscillator quadratures, whose covariance matrix is determined by the Riccati equation in a steady state. We derived the logarithmic negativity for the X and Y measurements in an analytic manner, including detuning and feedback control, and are not limited to only the free-mass regions.

We analyzed the logarithmic negativity and phase space distribution, assuming tabletop experiments with the experimentally feasible parameters expected from the present technique [5, 6]. The quantum cooperativity  $C_{\pm}/n_{\text{th}}^{\pm}$  and the detuning  $\delta_{\pm}$  characterize the entanglement behavior. The common mode and the differential mode of the oscillators are quantum-squeezed for  $C_{\pm}/n_{\text{th}}^{\pm} \gtrsim 1$ , however, it is not enough for entanglement generation. Namely, entanglement does not occur in the region with low purity even if both modes are squeezed. Therefore, quantum-squeezed states with high purity are necessary to generate entanglements. The required values for generating the entanglement depend on the detuning and measurement schemes. For the X measurement, the condition of the quantum cooperativity  $C_-/n_{\text{th}}^- \gtrsim 3$  is required, assuming  $\zeta = 3$  and  $\delta_- = 0.2$ . These values will be achieved in the mid-term. The required values for the Y measurement can be slightly weakened depending on the level of detuning applied, though the homodyne (Y) measurement with high-power laser is experimentally difficult to achieve. Thus, it is possible to experimentally generate quantum entanglement between mg-scale objects in the near future. These predictions of quantum entanglement between macroscopic objects are not only a first step towards verifying the quantum nature of gravity but may also assist in verifying quantum mechanics in the macroscopic world.

For a realistic experimental setup, there are issues to be further considered. In the present analysis, coating thermal noise is ignored. This approximation is typically valid for the bandwidth around 1 kHz [5], but the influence of such

a noise should be clarified in wide parameter regions. In an optomechanics with suspended mirrors, there exists additional mechanical modes other than the pendulum mode, e.g., rotation mode and violin modes [38], which is also left as future investigations.

## ACKNOWLEDGMENTS

We are grateful for the discussions in the QUP theoretical collaboration. We especially thank S. Iso for his support and helpful discussions. K.Y. was partially supported by JSPS KAKENHI, Grant No. 22H05263. N.M. is supported by JSPS KAKENHI, Grant No. 19H00671 and JST FORESTO, Grant NO. JPMJFR202X. D.M. is supported by JSPS KAKENHI, Grant No. 22J21267.

## Appendix A: Derivation of the Basic Equations – BACKGROUND AND PERTURBATION –

### 1. INDIVIDUAL OSCILLATOR AND CAVITY PHOTONS

The Hamiltonian for the two oscillators and cavities is given by:

$$H = \frac{\hbar\Omega}{4}(q_1^2 + p_1^2) + \frac{\hbar\Omega}{4}(q_2^2 + p_2^2) + \hbar\omega_c a_1^\dagger a_1 + \hbar\omega_c a_2^\dagger a_2 \\ + \hbar G q_1 a_1^\dagger a_1 + \hbar G q_2 a_2^\dagger a_2 + i\hbar E (a_1^\dagger e^{-i\omega_L t} - a_1 e^{i\omega_L t}) + i\hbar E (a_2^\dagger e^{-i\omega_L t} - a_2 e^{i\omega_L t}), \quad (\text{A1})$$

where  $[q_1, p_1] = [q_2, p_2] = 2i$ ,  $[a_1, a_1^\dagger] = [a_2, a_2^\dagger] = 1$ ,  $G = (\omega_c/\ell)\sqrt{\hbar/2m\Omega}$ , and we assume that the incident laser on each cavity has the same  $E = \sqrt{P_{\text{in}}\kappa/\hbar\omega_L}$ . The Langevin equations are given by:

$$\dot{q}_i = \Omega p_i, \\ \dot{p}_i = -\Omega q_i - 2G a_i'^\dagger a_i' - \Gamma p_i + \sqrt{2\Gamma} p_{\text{in}}, \\ \dot{a}_i' = i(\omega_L - \omega_c) a_i' - iG q_i a_i' + E - \frac{\kappa}{2} a_i' + \sqrt{\kappa} a_{\text{in}}^i, \quad (\text{A2})$$

where  $i = 1$  or  $2$  and  $a' = e^{i\omega_L t} a$ . Henceforth, we denote  $a'$  as  $a$ . Considering the linearization  $q \rightarrow \bar{q} + q$ ,  $p \rightarrow \bar{p} + p$ , and  $a \rightarrow \bar{a} + a$ , we derive the following background equations:

$$\dot{\bar{q}}_i = \Omega \bar{p}_i, \\ \dot{\bar{p}}_i = -\Omega \bar{q}_i - 2G |\bar{a}_i|^2 - \Gamma \bar{p}_i, \\ \dot{\bar{a}}_i = i(\omega_L - \omega_c - G \bar{q}_i) \bar{a}_i + E - \frac{\kappa}{2} \bar{a}_i. \quad (\text{A3})$$

Here, we assume that the background is in a steady state  $\dot{\bar{q}}_i = \dot{\bar{p}}_i = \dot{\bar{a}}_i = 0$ . The background equations are then rewritten as:

$$\bar{q}_1 = -2\frac{G}{\Omega} |\bar{a}_1|^2, \quad \bar{q}_2 = \bar{q}_1, \\ \bar{p}_1 = 0, \quad \bar{p}_2 = 0, \\ \bar{a}_1 = \frac{2E}{\kappa - 2i\Delta}, \quad \bar{a}_2 = \bar{a}_1, \quad (\text{A4})$$

where we define the detuning  $\Delta = \omega_L - \omega_c + 2(G|\bar{a}_1|)^2/\Omega$ . The perturbation equations are as follows:

$$\dot{q}_i = \Omega p_i, \\ \dot{p}_i = -\Omega q_i - 2G(\bar{a}_i^* a_i + \bar{a}_i a_i^\dagger) - \Gamma p_i + \sqrt{2\Gamma} p_{\text{in}}^i, \\ \dot{a}_i = i\Delta a_i - iG \bar{a}_i q_i - \frac{\kappa}{2} a_i + \sqrt{\kappa} a_{\text{in}}^i. \quad (\text{A5})$$

## 2. COMMON AND DIFFERENTIAL MODES

We consider the Fabry-Perot-Michelson interferometer shown in Fig. 1. By introducing the common and differential modes  $q_{\pm} = (q_1 \pm q_2)/\sqrt{2}$ ,  $p_{\pm} = (p_1 \pm p_2)/\sqrt{2}$ ,  $a_{\pm} = (a_1 \pm a_2)/\sqrt{2}$ , the Hamiltonian is

$$H = \frac{\hbar\Omega}{4}(q_+^2 + p_+^2) + \frac{\hbar\Omega}{4}(q_-^2 + p_-^2) + \hbar\omega_c a_+^\dagger a_+ + \hbar\omega_c a_-^\dagger a_- \\ + \hbar\frac{G}{\sqrt{2}}q_+(a_+^\dagger a_+ + a_-^\dagger a_-) + \hbar\frac{G}{\sqrt{2}}q_-(a_+^\dagger a_- + a_+ a_-^\dagger) + i\hbar E_+(a_+^\dagger e^{-i\omega_L t} - a_+ e^{i\omega_L t}), \quad (\text{A6})$$

where  $E_+ = \sqrt{P_{\text{in}}\kappa_+/\hbar\omega_L}$  denotes the input laser amplitude in the common-side cavity. The Langevin equations are written as follows:

$$\dot{q}_{\pm} = \Omega p_{\pm}, \\ \dot{p}_{\pm} = -\Omega q_{\pm} - 2G(a_+^\dagger a_{\pm} \pm a_-^\dagger a_{\mp})/\sqrt{2} - \Gamma p_{\pm} + \sqrt{2\Gamma}p_{\text{in}}^{\pm}, \\ \dot{a}_+ = i(\omega_L - \omega_c)a_+ - iG(q_+ a_+ + q_- a_-)/\sqrt{2} - \frac{\kappa_+}{2}a_+ + \sqrt{\kappa_+}a_{\text{in}}^+ + E_+, \\ \dot{a}_- = i(\omega_L - \omega_c)a_- - iG(q_+ a_- - q_- a_+)/\sqrt{2} - \frac{\kappa_-}{2}a_- + \sqrt{\kappa_-}a_{\text{in}}^-. \quad (\text{A7})$$

Considering the linearization of each quadrature, we derive the background equations as:

$$\dot{\bar{q}}_{\pm} = \Omega \bar{p}_{\pm}, \\ \dot{\bar{p}}_{\pm} = -\Omega \bar{q}_{\pm} - \sqrt{2}G(\bar{a}_+^* \bar{a}_{\pm} + \bar{a}_-^* \bar{a}_{\mp}) - \Gamma \bar{p}_{\pm}, \\ \dot{\bar{a}}_+ = i(\omega_L - \omega_c)\bar{a}_+ - iG(\bar{q}_+ \bar{a}_+ + \bar{q}_- \bar{a}_-)/\sqrt{2} - \frac{\kappa_+}{2}\bar{a}_+ + E_+, \\ \dot{\bar{a}}_- = i(\omega_L - \omega_c)\bar{a}_- - iG(\bar{q}_+ \bar{a}_- + \bar{q}_- \bar{a}_+)/\sqrt{2} - \frac{\kappa_-}{2}\bar{a}_-. \quad (\text{A8})$$

Here, we assume that the background is in a steady state  $\dot{\bar{q}}_{\pm} = \dot{\bar{p}}_{\pm} = \dot{\bar{a}}_{\pm} = 0$ . Assuming that the individual background quadratures are equal to  $\bar{q}_1 = \bar{q}_2$ ,  $\bar{p}_1 = \bar{p}_2$ ,  $\bar{a}_1 = \bar{a}_2$ , the background quadratures of the differential mode are zero  $\bar{q}_- = \bar{p}_- = \bar{a}_- = 0$ . Hence, equation (A8) can be rewritten as:

$$\bar{q}_+ = \sqrt{2}\bar{q}_1 = -\frac{\sqrt{2}G|\bar{a}_+|^2}{\Omega}, \quad \bar{q}_- = 0, \\ \bar{p}_{\pm} = 0, \\ \bar{a}_+ = \sqrt{2}\bar{a}_1 = \frac{2E_+}{\kappa_+ - 2i\Delta_+}, \quad \bar{a}_- = 0, \quad (\text{A9})$$

where we define detuning as:

$$\Delta_+ = \omega_L - \omega_c - \frac{G}{\sqrt{2}}\bar{q}_+ \\ = \omega_L - \omega_c + \frac{G^2}{\Omega}|\bar{a}_+|^2 \\ = \omega_L - \omega_c + 2\frac{G^2}{\Omega}|\bar{a}_1|^2 = \Delta. \quad (\text{A10})$$

Then, the perturbation equations are:

$$\dot{q}_{\pm} = \Omega p_{\pm}, \\ \dot{p}_{\pm} = -\Omega q_{\pm} - 2g_+(e^{-i\phi} a_{\pm} + e^{i\phi} a_{\pm}^\dagger) - \Gamma p_{\pm} + \sqrt{2\Gamma}p_{\text{in}}^{\pm}, \\ \dot{a}_{\pm} = i\Delta a_{\pm} - ig_+ e^{i\phi} q_{\pm} - \frac{\kappa_{\pm}}{2}a_{\pm} + \sqrt{\kappa_{\pm}}a_{\text{in}}^{\pm}, \quad (\text{A11})$$

where  $\bar{a}_+ = |\bar{a}_+|e^{i\phi}$  and the optomechanical coupling is

$$g_+ = |\bar{a}_+|G/\sqrt{2} \\ = |\bar{a}_1|G = g. \quad (\text{A12})$$

The parameters have the same forms as the individual case except for the optical decay rates, and the equations are also in the same form as Eqs. (4) in Sec. II. Hence, we derived the covariance matrix for the common and differential modes in the same manner.



### Appendix B: LOGARITHMIC NEGATIVITY

Using the quality factor  $Q_{\pm} = \omega_m^{\pm}/\gamma_m$  and cooperativity  $C_{\pm} = 4(g_m^{\pm})^2/\gamma_m\kappa_{\pm}$ , we obtain

$$\frac{\lambda_X^{\pm}}{\gamma_m} = \frac{16C_{\pm}\delta_{\pm}^2\eta}{(2\eta N_{\text{th}} + 1)(1 + 4\delta_{\pm}^2)^2} \equiv \lambda_X^{\pm'}, \quad \frac{\lambda_Y^{\pm}}{\gamma_m} = \frac{4C_{\pm}\eta}{(2\eta N_{\text{th}} + 1)(1 + 4\delta_{\pm}^2)^2} \equiv \lambda_Y^{\pm'}, \quad (\text{B1})$$

$$\frac{\Lambda_X^{\pm}}{\gamma_m} = -\frac{\Lambda_Y^{\pm}}{\gamma_m} = -\frac{8C_{\pm}\delta_{\pm}\eta}{(1 + 4\delta_{\pm}^2)^2} \frac{2N_{\text{th}} + 1}{2\eta N_{\text{th}} + 1} \equiv \Lambda_X^{\pm'}, \quad (\text{B2})$$

$$\frac{\bar{n}_{\pm}}{\gamma_m} = 4n_{\text{th}}^{\pm} + 2 + \frac{4C_{\pm}}{(1 + 4\delta_{\pm}^2)}(2N_{\text{th}} + 1) \equiv \bar{n}'_{\pm}, \quad (\text{B3})$$

$$\frac{\gamma_I^{\pm}}{\gamma_m} = \sqrt{1 - 2Q_{\pm}^2 \left( 1 + \frac{\Lambda_I^{\pm}}{\gamma_m Q_{\pm}} - \sqrt{1 + 2\frac{\Lambda_I^{\pm}}{\gamma_m Q_{\pm}} + \frac{\bar{n}_{\pm}\lambda_I^{\pm}}{\gamma_m^2 Q_{\pm}^2}} \right)} \equiv \gamma_I^{\pm'}, \quad (\text{B4})$$

where we define  $\delta_{\pm} = \Delta/\kappa_{\pm}$ . From Eqs. (49) and (50), we exactly derive the critical value as:

$$\epsilon_{\text{cr}} = -\frac{1}{2}\log_2 \left[ \frac{(\gamma_I^{+'} - 1)(\gamma_I^{-'} - 1)}{4\lambda_I^{+'}\lambda_I^{-'}} \left\{ \left( \frac{(\gamma_I^{+'})^2 + (\gamma_I^{-'})^2 - \gamma_I^{+'}\gamma_I^{-'} - 1}{Q_+Q_-} + 2\frac{\Lambda_I^{+'} + Q_+}{Q_-} + 2\frac{\Lambda_I^{-'} + Q_-}{Q_+} \right) \right. \right. \\ \left. \left. - \left( \frac{((\gamma_I^{+'})^2 + (\gamma_I^{-'})^2 - 1)(\gamma_I^{+'} - \gamma_I^{-'})^2}{Q_+^2 Q_-^2} + 4 \left( \frac{\Lambda_I^{+'} + Q_+}{Q_-} - \frac{\Lambda_I^{-'} + Q_-}{Q_+} \right)^2 \right) \right. \right. \\ \left. \left. + 4 \frac{\gamma_I^{+'}(\gamma_I^{+'} - \gamma_I^{-'})(\Lambda_I^{+'} + Q_+)}{Q_+ Q_-^2} - 4 \frac{\gamma_I^{-'}(\gamma_I^{-'} - \gamma_I^{+'})(\Lambda_I^{-'} + Q_-)}{Q_+^2 Q_-} \right\}^{1/2} \right]. \quad (\text{B5})$$

### Appendix C: SQUEEZING ANGLE

The covariance matrix of a single mirror is diagonalized as:

$$\mathbf{V} = P^{-1} \begin{pmatrix} \frac{1}{2}(V_{11} + V_{22} - \sqrt{(V_{11} - V_{22})^2 + 4V_{12}^2}) & 0 \\ 0 & \frac{1}{2}(V_{11} + V_{22} + \sqrt{(V_{11} - V_{22})^2 + 4V_{12}^2}) \end{pmatrix} P \quad (\text{C1})$$

with

$$P = \begin{pmatrix} \sqrt{\frac{1}{2} \left( 1 + \frac{-V_{11} + V_{22}}{\sqrt{(V_{11} - V_{22})^2 + 4V_{12}^2}} \right)} & \sqrt{\frac{1}{2} \left( 1 - \frac{-V_{11} + V_{22}}{\sqrt{(V_{11} - V_{22})^2 + 4V_{12}^2}} \right)} \\ -\sqrt{\frac{1}{2} \left( 1 - \frac{-V_{11} + V_{22}}{\sqrt{(V_{11} - V_{22})^2 + 4V_{12}^2}} \right)} & \sqrt{\frac{1}{2} \left( 1 + \frac{-V_{11} + V_{22}}{\sqrt{(V_{11} - V_{22})^2 + 4V_{12}^2}} \right)} \end{pmatrix}, \quad (\text{C2})$$

where  $P$  is the rotation matrix, and its components are defined as:

$$P = \begin{pmatrix} \cos(-\theta) & -\sin(-\theta) \\ \sin(-\theta) & \cos(-\theta) \end{pmatrix}. \quad (\text{C3})$$

Hence, the squeezing angle can be obtained as follows:

$$\theta = \arctan \left[ \frac{\sqrt{\sqrt{(V_{22} - V_{11})^2 + 4V_{12}^2} + V_{11} - V_{22}}}{\sqrt{\sqrt{(V_{22} - V_{11})^2 + 4V_{12}^2} - V_{11} + V_{22}}} \right] = \arctan \left[ \frac{\sqrt{V_{11} - E_{\text{min}}}}{E_{\text{max}} - V_{11}} \right], \quad (\text{C4})$$

where  $E_{\text{min}}$  ( $E_{\text{max}}$ ) denotes the minimum (maximum) eigenvalue of the covariance matrix  $\mathbf{V}_{\pm}$ .

- 
- [1] M. Aspelmeyer, T. J. Kippenberg, and F. Marquardt, Cavity optomechanics, *Rev. Mod. Phys.* **86**, 1391 (2014)
- [2] Y. Chen, Macroscopic quantum mechanics; theory and experimental concepts of optomechanics, *J. Phys. B: At. Mol. Opt. Phys.* **46** 104001 (2013)
- [3] W. P. Bowen, G. J. Bilburn, *Quantum Optomechanics*, (CRC Press, 2015)
- [4] N. Matsumoto, S. B. Cataño-Lopez, M. Sugawara, and S. Suzuki, Demonstration of Displacement Sensing of a mg-Scale Pendulum for mm- and mg-Scale Gravity Measurements, *Phys. Rev. Lett.* **122**, 071101 (2019)
- [5] S. B. Cataño-Lopez, J. G. Santiago-Condori, K. Edamatsu, N. Matsumoto, High-Q Milligram-Scale Monolithic Pendulum for Quantum-Limited Gravity Measurements, *Phys. Rev. Lett.* **124**, 221102, (2020)
- [6] N. Matsumoto and N. Yamamoto, Preparing mechanical squeezing of a macroscopic pendulum near quantum regimes, arXiv:2008.10848
- [7] C. Meng, G. A. Brawley, J. S. Bennett, M. R. Vanner, and W. P. Bowen, Mechanical Squeezing via Fast Continuous Measurement, *Phys. Rev. Lett.* **125**, 043604 (2020)
- [8] C. Genes, et al., *Phys. Rev. A* **77** 033804 (2008)
- [9] D. Vitali, et al., *Phys. Rev. Lett.* **98** 030405 (2007)
- [10] H. Miao, S. Danilishin, H. Müller-Hbhardt, Y. Chen, *New Journal of Physics*, **12** (2010) 083032
- [11] C. F. Ockeloen-Korppi, E. Damskägg, J. -M. Pirkkalainen, M. Asjad, A. A. Clerk, F. Massel, M. J. Woolley, and M. A. Sillanpää, Stabilized entanglement of massive mechanical oscillators, *Nature* **556**, 478–482 (2018)
- [12] S. Kotler, G. A. Peterson, E. Shojaei, F. Lecocq, K. Cicak, A. Kwiatkowski, S. Geller, S. Glancy, E. Knill, R. W. Simmonds, J. Aumentado, and J. D. Teufel, Direct observation of deterministic macroscopic entanglement, *Science* **372**, 622–625 (2021)
- [13] L. Mercier de Lépinay, C. F. Ockeloen-Korppi, M. J. Woolley, and M. A. Sillanpää, Quantum mechanics-free subsystem with mechanical oscillators, *Science* **372**, 625–629 (2021)
- [14] A. A. Balushi, W. Cong, and R. B. Mann, *Phys. Rev. A* **98** 043811 (2018)
- [15] H. Miao, D. Martynov, H. Yang, and A. Datta, Quantum correlations of light mediated by gravity, *Phys. Rev. A* **101** 063804 (2020)
- [16] A. Matsumura and K. Yamamoto, *Phys. Rev. D* **102** 106021 (2020)
- [17] T. Krisnanda, G. Y. Tham, M. Paternostro, and T. Paterek, *Quantum Inf.* **6**, 12 (2020)
- [18] A. Datta and H. Miao, Signatures of the quantum nature of gravity in the differential motion of two masses, *Quantum Sci. Technol.* **6**, 045014 (2021)
- [19] D. Miki, A. Matsumura, and K. Yamamoto, *Phys. Rev. D* **105** (2022) 026011
- [20] A. D. K. Plato, D. Rätzel, and C. Wan, arXiv:2209.12656
- [21] S. Bose, A. Mazumdar, G. W. Morley, H. Ulbricht, M. Toroš, M. Paternostro, A. A. Geraci, P. F. Barker, M. S. Kim, and G. Milburn, *Phys. Rev. Lett.* **119** 240401 (2017)
- [22] C. Marletto and V. Vedral, *Phys. Rev. Lett.* **119** 240402 (2017)
- [23] D. Carney, Newton, entanglement, and the graviton, *Phys. Rev. D* **105**, 024029 (2022)
- [24] S. Bose, A. Mazumdar, M. Schut, and M. Toroš, Mechanism for the quantum natured gravitons to entangle masses, arXiv:2201.03583
- [25] A. Belenchia, R. M. Wald, F. Giacomini, E. Castro-Ruiz, Č. Brukner, and M. Aspelmeyer, Quantum superposition of massive objects and the quantization of gravity, *Phys. Rev. D* **98**, 126009 (2018)
- [26] D. L. Danielson, G. Satishchandran, and R. M. Wald, Gravitationally Mediated Entanglement: Newtonian Field vs. Gravitons, *Phys. Rev. D* **105**, 086001 (2022)
- [27] R.J. Marshman, A. Mazumdar, and S. Bose, Locality and entanglement in table-top testing of the quantum nature of linearized gravity, *Phys. Rev. A* **101**, 052110 (2020)
- [28] A. Belenchia, R. M. Wald, F. Giacomini, E. Castro-Ruiz, C. Brukner, and M. Aspelmeyer, Quantum superposition of massive objects and the quantization of gravity, *Phys. Rev. D* **98**, 126009 (2018)
- [29] H. Chau Nguyen and F. Bernards, Entanglement dynamics of two mesoscopic objects with gravitational interaction, *Eur. Phys. J. D* **74**, 69 (2020)
- [30] D. Miki, A. Matsumura, and K. Yamamoto, Entanglement and decoherence of massive particles due to gravity, *Phys. Rev. D* **103**, 026017 (2021)
- [31] A. Matsumura, Field-induced entanglement in spatially superposed objects, *Phys. Rev. D* **104**, 046001 (2021)
- [32] Y. Sugiyama, A. Matsumura, and K. Yamamoto, Effects of photon field on entanglement generation in charged particles, *Phys. Rev. D* **106**, 045009 (2022)
- [33] Y. Sugiyama, A. Matsumura, and K. Yamamoto, Consistency between causality and complementarity guaranteed by Robertson inequality in quantum field theory, arXiv:2206.02506
- [34] A. Matsumura, Y. Nambu, and K. Yamamoto, Leggett-Garg inequalities for testing quantumness of gravity, *Phys. Rev. A* **106**, 012214 (2022)
- [35] T. Feng and V. Vedral, Amplification of Gravitationally induced Entanglement, arXiv:2202.09737
- [36] A. Matsumura, Role of matter coherence in entanglement due to gravity, arXiv:2204.00324
- [37] H. Müller-Hebhardt, H. Rehbeim, R. Schnabel, K. Danzmann, and Y. Chen, *Phys. Rev. Lett.* **100**, 013601 (2008)
- [38] G. I. Gonzalez, P. R. Saulson, *J. Acoust. Soc. Am.* **96**, 207 (1994)